ELSEVIER

Selective imaging probes for differential detection of pathological tau polymorphs in tauopathies

Nicolò Bisi *, **Luca Pinzi**, **Giulio Rastelli**

Department of Life Sciences, University of Modena and Reggio Emilia, Via Giuseppe Campi 103, 41125 Modena, Italy

Tauopathies, including Alzheimer's disease (AD), Pick's disease (PiD), progressive supranuclear palsy (PSP) and corticobasal degeneration (CBD), are characterized by the misfolding and pathological aggregation of the tau protein, leading to neurodegeneration. Although the pathogenesis of these diseases is still a matter for debate, the formation of amyloid inclusions still represents the only histopathological hallmark available. Tau inclusions are not the same in terms of structure and morphology, and different tauopathies are characterized by different polymorphs. Remarkably, the selective detection of these polymorphs is crucial for differential diagnosis, disease monitoring and evaluation of the potential harmfulness of polymorphs, with a significant impact on drug discovery. This review discusses recent advances in the development of imaging probes designed for the selective detection of pathological tau forms associated with specific tauopathies. We explore the application of compounds that can target tau polymorphs characteristic of AD, PiD, PSP and CBD. In particular, we focus on discussing the probes' selectivity and sensitivity in distinguishing between the different tauopathy-associated polymorphs in preclinical settings. The progress and the weaknesses in this field are discussed, to guide the researchers in identifying accurate and potent probes for the selective diagnosis of these different neurodegenerative diseases.

Nicolò Bisi is a post-doctoral researcher at University of Modena and Reggio Emilia, specializing in the design, synthesis and evaluation of anticancer and anti-neurodegenerative drug candidates, working in the team of Prof. Giulio Rastelli. He earned his PhD from Université Paris-Saclay (Prof. Sandrine Ongeri) and Osnabruck University (Prof. Roland Brandt) in July 2024 through a European Joint Doctorate program (TublnTrain), focusing on the design, synthesis and evaluation of α-synuclein and tau aggregation inhibitors. After his PhD, he specialized in the field of peptide and peptidomimetics synthesis thanks to his first post-doctoral fellowship at the Vrije Universiteit Brussel under the supervision of Prof. Steven Ballet.

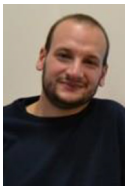

Luca Pinzi is a dedicated fixed-term assistant professor at University of Modena and Reggio Emilia, within the area of medicinal chemistry. He achieved his MSc (February 2014) in medicinal chemistry and pharmaceutical technology and his second-level Master's degree (October 2014) in drug design and synthesis at the University of Siena. Afterward, he obtained his PhD (March 2018) in clinical and experimental medicine at the University of Modena and Reggio Emilia. His expertise is in the fields of drug discovery, molecular modeling, drug design, docking, molecular docking, cheminformatics and computational chemistry, as well as virtual screening.

Giulio Rastelli is a professor of medicinal chemistry and head of the Molecular Modeling & Drug Design Laboratory of the University of Modena and Reggio Emilia. He received his PhD in medicinal chemistry from the University of Modena and Reggio Emilia and has been a research fellow at the University of California San Francisco under the supervision of Daniel Santi and Peter Kollman. His research interests focus on the development and application of computational drug design methodologies. He collaborates with academic and private institutions for the discovery and development of small-molecule inhibitors of relevant drug targets, with a special focus on cancer.

* *Corresponding author. Bisi, N. (nicobisi@unimore.it)*

https://doi.org/10.1016/j.drudis.2025.104352

Introduction

Tauopathies are known as age-related, neurodegenerative disorders characterized by the pathological accumulation of tau protein in the brain.[p1],[p2],[p3] The four main tauopathies in terms of prevalence and sanitary burden are Alzheimer's disease (AD), Pick's disease (PiD), progressive supranuclear palsy (PSP) and corticobasal degeneration (CBD), the last three being part of the frontotemporal dementia (FTLD) group.[p4] Currently, AD accounts for >60% of all tauopathy cases, bearing a tremendous socioeconomic burden worldwide. More than 55 million people worldwide suffer from AD, with 6 million cases in America and 5 million in Europe, with a financial cost for hospitalization and treatment of US$259 billion.[p5] Tau is a microtubule-associated protein (MAP) that regulates and intervenes in physiological microtubule dynamics.[p2],[p6] Under pathological conditions observed in tauopathies, the protein tau misfolds and aggregates, while undergoing a hyperphosphorylation process.[p7],[p8],[p9],[p10] This eventually leads to neurodegeneration and neuronal death, with tau encountering a loss-of-function and gain-of-toxic-function.[p11],[p12] In fact, the MAP is no more able to properly intervene in MT dynamics, thus leading to cytoskeleton impairment, as well as the formation of toxic oligomers and fibrils responsible for the cell death.[p13],[p14],[p15],[p16] Although the literature remains controversial about which species of aggregated tau is the most toxic,[p17],[p18] the inclusions found in patient brains are the only histopathological markers nowadays associated with tauopathies.[p19],[p20],[p21]

Tau structure and tauopathies

Four main regions can be identified in the structure of tau. In particular, tau presents an N-terminal region (NTR), a microtubule-binding region (MBR), a proline-rich region (PRR) and a C-terminal region (CTR; Figure 1).[p22],[p23] The NTR (1–165 for tau N2R4; Figure 1) takes part in several functions, such as microtubule dynamics regulation and cell-signaling pathways, and is also involved in protein–protein interactions (PPIs). When tau binds to microtubules, the NTR extends outside the MT surface and interacts with other proteins such as annexins, via electrostatic interactions, because the NTR is negatively charged owing to the various glutamate and aspartate residues.[p24] The truncation of tau NTR generates constructs of the protein responsible for tau pathology, like Gln124-tau.[p25] The PRR region (sequence 166–242 for tau N2R4; Figure 1) presents a large number of proline, serine and threonine residues. It contributes to the regulation of tau's interaction with microtubules, by modulating the protein-binding affinity. In particular, this region influences the interaction of tau on the microtubule surface, affecting microtubule dynamics.[p26] These interactions are important for tau's role in signal transduction pathways that regulate cytoskeletal dynamics and cellular responses to external stimuli. Because this region bears a large number of residues prone to phosphorylation, the PRR is an intriguing target for therapeutic intervention. Abnormal phosphorylation in the PRR is commonly observed in pathologies like AD, where it contributes to the detachment of tau from microtubules and its subsequent aggregation into neurofibrillary tangles (NFTs).[p27] The peculiar structure provided by proline residues allows the PRR to adopt different conformations, which can facilitate or inhibit the formation of toxic tau aggregates. In particular, this can also influence the type of tau aggregates formed, which varies across different tauopathies (e.g., AD, PSP and CBD).[p28]

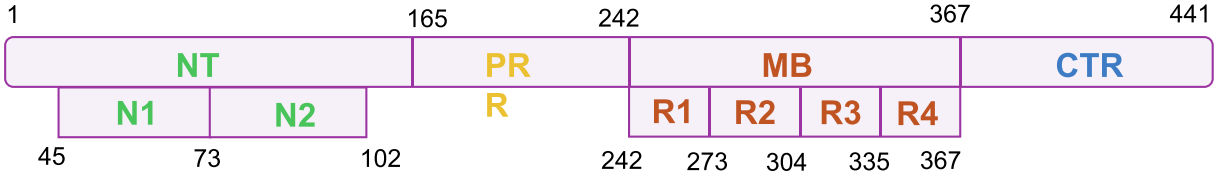

Tau region	Residues	Function
NTR	1–165	MT dynamics regulation, cell signaling, PPI, tau signaling, PPI, tau function regulation (truncation: regulation (truncation: tauoapathy)
PRR	166–242	MT and cytoskeleton dynamics regulation, kinase
MBR	243–367	MT binding, PPI (chaperones, actin and and amyloids)
CTR	368–441	PPI, tau function regulation (truncation: (truncation: tauopathy)

Drug Discovery Today

FIGURE 1

Tau's different domains and functions, according to the primary structure of the longest tau isoform 2NR4. The various regions of the protein, as well as their residue numbers are depicted in the figure. Also, their main functions are presented.

The MBR region of tau (residues 243–367 for tau N2R4; Figure 1) has a central role in the interaction with microtubules, which probably occurs through the establishment of several electrostatic interactions between the positively charged lysines of the MBR and the negatively charged surface of microtubules.[p29] The MBR is also important for PPI, because it interconnects with chaperones and actin. Notably, the MBR is also involved in amyloid–amyloid interaction, being responsible for co-morbidities in, for example, Parkinson's disease. In this case, tau's MBR is thought to interact with the negatively-charged C-terminal domain of α-synuclein, synergically driving the formation of tau and α-synuclein aggregates.[p30],[p31],[p32],[p33],[p34],[p35],[p36],[p37],[p38] Importantly, MBR is also sensitive to phosphorylation, in particular on residues 258, 262, 289 and 356.[p39] Regarding the last region of the tau structure, namely the CTR (368–441 for tau N2R4; Figure 1), its role is mainly related to PPI and tau's physiological function preservation. In fact, several CTR truncation constructs (e.g., tau-421, tau-368, tau-397 and tau-422) are shown to induce tau pathology in cellular and *in vivo* models.[p40],[p41],[p42]

Six tau isoforms are present in the central nervous system (CNS), which differ for the N-terminal inserts (0N, 1N, 2N) and the repeats present in the MBR (3R or 4R). Of note, the number of repeats present in the tau MBR influences the affinity of the protein for MTs, with tau 4R showing the highest affinity.[p43] One criteria that discriminates the different tauopathies is the number of repeats present in the tau MBR. In this review, we focus on the four main tauopathies in terms of prevalence and sanitary burden (AD, PiD, PSP and CBD). AD is associated with the accumulation of all six tau isoforms (3R and 4R-tau), where the misfolded and aggregated protein forms paired helical filaments (PHFs) and straight filaments (SFs).[p18],[p44],[p45],[p46] The aggregates form neurofibrillary tangles (NFTs) primarily in the hippocampus and cerebral cortex.[p47] PiD is associated with the accumulation of three-repeat tau isoforms (3R-tau). These aggregates form in Pick bodies, which are spherical inclusions found in neurons. PiD typically affects the frontal and temporal lobes, leading to symptoms such as behavioral changes, language difficulties and progressive dementia.[p48],[p49] PSP is characterized by the accumulation of 4R-tau. These aggregates form in tufted astrocytes, coiled bodies and globose NFTs primarily in the basal ganglia, brainstem and cerebellum. PSP is known for its early onset of postural instability, gaze palsy and cognitive impairment.[p50],[p51] CBD, instead, is characterized by the accumulation of 4R-tau isoforms. The aggregates form in astrocytic plaques, corticobasal bodies and neurofibrillary tangles. CBD primarily affects the cerebral cortex and basal ganglia, leading to symptoms such as asymmetric motor dysfunction and cognitive decline.[p52],[p53] Table 1[p54],[p55],[p56],[p57],[p58],[p59] reports the different R-tau isoforms associated with these four tauopathies, along with the respective localization of tau inclusions.

Polymorphism in tau aggregates

Recent advances in experimental spectroscopy (e.g., with the introduction of cryogenic electron microscopy, or cryo-EM) has enabled the analysis and characterization of tau filaments at atomic levels, and the comparison of their structure across different tauopathies.[p45],[p60],[p61],[p62] Under pathological conditions, tau forms toxic inclusions differing in shape, morphology and size. Tau polymorphism in tauopathies refers to the various structural forms that tau aggregates can adopt. These structural differences are the result of variations in how tau protein molecules fold, pack and assemble into fibrils, which are consistent among individuals with the same disease, leading to distinct pathological features.[p60] In AD, tau aggregates form PHFs and SFs. PHFs are characterized by a twisted, helical structure,[p45] whereas SFs, which share a similar core structure with PHFs, differ for their straight, non-twisted morphology.[p63] The polymorphism between PHFs and SFs can be attributed to differences at the protofilament interface, with PHFs exhibiting symmetric interfaces stabilized by H-bonds, whereas SFs display asymmetric arrangements without such stabilizing interactions (Figure 2). The co-existence of these two types of aggregates within the same disease condition highlights the structural polymorphism of tau in AD.[p60],[p63]

In PSP, tau aggregates mostly form SFs (Figure 2). These aggregates have a unique core structure that differs significantly from the PHFs and SFs seen in AD.[p64] Cryo-EM studies have shown that tau filaments in PSP are characterized by a distinct fold involving residues 274–380, with a compact and symmetric structure. This fold is specific to PSP aggregates and is not found in other tauopathies.[p64] Notably, CBD is associated with tau aggregates that adopt a ribbon-like structure (Figure 2).[p52],[p53],[-

TABLE 1

Different tau isoforms (3R or 4R) associate with different tauopathies; depending on the tau pathology, the localization of the amyloid aggregates varies as well.

Tauopathy	Aggregate type	Tau isoforms (3R or 4R)	Aggregate localization	Type of cells
AD	Neurofibrillary tangles	3R and 4R	Hippocampus, cerebral cortex	Neurons and glial cells[p54],[p55]
PiD	Pick bodies	3R	Frontal and temporal lobes	Neurons and glial cells[p56]
PSP	Tufted astrocytes, coiled bodies, globose neurofibrillary tangles	4R	Basal ganglia, brainstem, cerebellum	Neurons, astrocytes and oligodendroglia[p57],[p58]
CBD	Astrocytic plaques, corticobasal bodies, neurofibrillary tangles	4R	Cerebral cortex, basal ganglia	Neurons (with corticobasal bodies in monoaminergic neurons), astrocytes and oligodendroglia[p58],[p59]

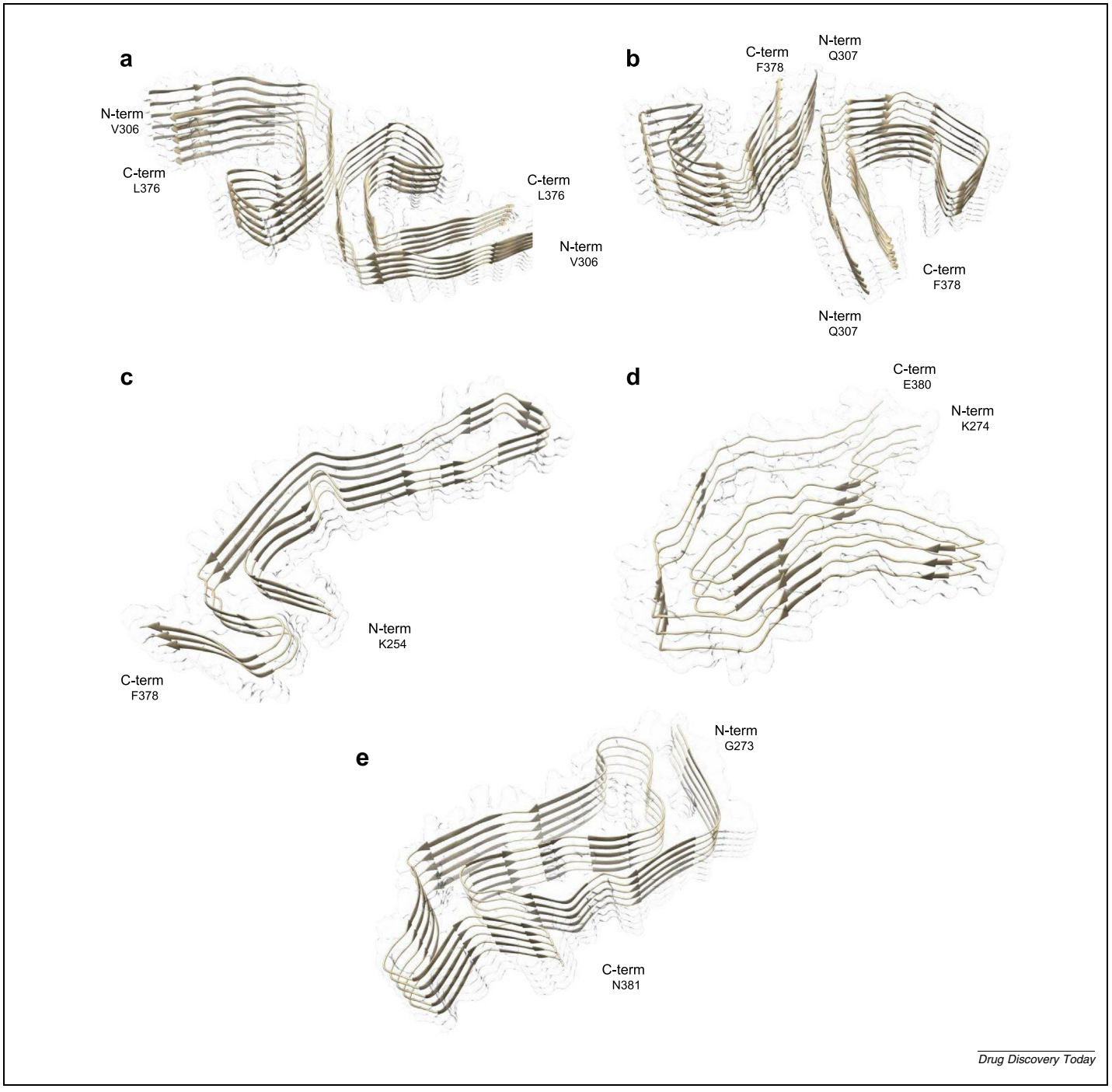

FIGURE 2

Selected 3D structures of: (i) PHFs (PDB code: 5O3L, panel **a**) and SFs (PDB code: 5O3T, panel **b**) of AD tau polymorphs[p45]; (ii) tau filaments from a patient with Pick's disease (PDB code: 6GX5, panel **c**)[p49]; (iii) a CBD tau filament (PDB code: 6TJO, panel **d**)[p53] and; (iv) a PSP tau filament (PDB code: 7P65, panel **e**).[p1]

[p59] The tau filaments in CBD are wider and less twisted than the PHFs of AD.[p53] The core of these filaments involves residues 274–380, similar to PSP, but the packing and overall morphology are distinct. CBD filaments are often described as twisted ribbons or wide filaments, reflecting their unique structural organization.[p53] In PiD, tau aggregates form spherical inclusions known as Pick bodies.[p49],[p56] The tau filaments within these inclusions have a unique structural fold, distinct from those seen in AD, PSP or CBD. The core of PiD tau filaments involves residues 254–380, with a distinctive β-helix-like structure that is not observed in other tauopathies.[p49] This unique fold contributes to the characteristic round shape of Pick bodies. Overall, the possibility of recognizing those different polymorphs could lead to an accurate early diagnosis of these different tauopathies. In this field,

imaging and fluorescent probes can play a pivotal part in discriminating the various polymorphs associated with the different tauopathies.

Molecular imaging and fluorescent probes to selectively recognize polymorphs in different tauopathies

The different polymorphism seen in tauopathies is one of the main criteria to discriminate among different tau diseases.[p65],[p66] However, only post-mortem analysis can accurately assess the kind of pathology suffered from patients.[p67],[p68] No early-diagnosis tool is available, and assessing the correct histopathological marker to a given tau pathology and *vice versa* is still far from being achieved. In this field, the use of fluorescent probes able to selectively bind to a polymorph characteristic of a determined tau pathology could represent a valuable solution to this challenge.[p69] Positron emission tomography (PET) still represents the main player in the detection of tauopathies (like AD) and amyloidosis, more generally. However, the diagnosis must be confirmed from post-mortem analysis.[p70],[p71],[p72] Also, most of the probes developed cannot discriminate among the different amyloid pathologies. Encouragingly, many efforts have been made in the field of bioimaging using non-invasive NIR probes in the frame of neurodegenerative diseases.[p73],[p74],[p75],[p76] Although these probes find application *in vitro*, their translation into clinical practice is still a challenge, often as a result of their unsuitable pharmacokinetic and safety profiles.[p69] Therefore, the exploration of new probes that selectively target tau polymorphs is a priority for future research. In the forthcoming sections, the scientific efforts made in the development of molecular imaging and fluorescent probes able to discriminate tau polymorphs in different tauopathies are described.

Alzheimer's disease

AD is a secondary or mixed tauopathy characterized by the co-occurrence of PHF and SF aggregates in brain cells.[p77] PHFs are characterized by a twisted, helical structure, with a periodicity of about 80 nm and a crossover distance between 650 and 800 Å.[p63] The PHF core consists of a series of β-sheets forming a C-shaped motif (residues V306–F378), encompassing R3 and R4 repeats and an additional C-terminal segment (residues

TABLE 2

Relevant tau PET probes reported in the literature: when present, the probe selectivity towards tau polymorphs and the mechanism of interaction are reported.

Compound ID	Tau polymorph selectivity	Mechanism of interaction	Type of detected tauopathy	Refs
[^{11}C]PBB3	NFTs, tufted astrocytes, astrocytic plaques, off-target activities	Not specified	AD, CBD, PSP, PiD	(p81),(p82),(p83),(p84)
[^{18}F]Flortaucipir (i.e., [^{18}F]AV-1451, [^{18}F]-T807, Tauvid)	PHFs, off-target activities	It binds within the C-shaped cavity of tau filaments of PHFs and SFs, inducing conformational changes[p85],[p86]	AD, CBD, PSP	(p84),(p87)
[^{18}F]T-808	PHFs, off-target activities	Not specified	AD	(p88)
[^{11}C]RO-643 (i.e., [^{11}C]RO-6924963)	NFTs	Not specified	AD	(p89)
[^{18}F]/[^{3}H]RO-948 (i.e., [^{18}F]/[^{3}H]-RO-6958948)	NFTs	Not specified	AD, PSP[p90]	(p89),(p91)
[^{11}C]RO-963 (i.e., [^{11}C]RO-6931643)	NFTs	Not specified	AD	(p89)
[^{18}F]Florzolotau (i.e., [^{18}F]PM-PBB3, [^{18}F]APN-1607)	PHFs and SFs (preferentially SFs)	It binds within the C-shaped cavity of tau filaments of PHFs and SFs, inducing conformational changes[p92]	AD, CBD, PSP, PiD	(p93)
[^{18}F]GTP-1	PHFs	It binds within the C-shaped cavity of tau filaments of PHFs[p94]	AD	(p95),(p96)
[^{18}F]JNJ-067 (i.e., [^{18}F]JNJ-64326067-AAA)	NFTs	Not specified	AD	(p97)
[^{18}F]JNJ-311	NFTs	Not specified	AD	(p98)
[^{18}F]SNFT-1	NFTs	Not specified	AD	(p99)
[^{18}F]/[^{3}H]MK-6240	PHFs, NFTs	It binds within the C-shaped cavity of tau filaments of PHFs	AD, PSP[p90]	(p86),(p91),(p100)
[^{18}F]/[^{3}H]PI-2620	PHFs	Not specified	AD, PSP,[p90] CBD	(p91),(p101),(p102)
[^{18}F]S16	NFTs	Not specified	AD	(p103)
[^{18}F]CBD-2115/[^{3}H]CBD-2115	Not specified	Not specified	AD, CBD, PSP	(p104)
THK compounds ([^{18}F]THK-523, [^{18}F]THK-5105, [^{18}F]THK-5116, [^{18}F]THK-5117 and [^{18}F]]/[^{3}H]THK-5351)	Several types of tau aggregates, off-target activities	Not specified	AD, CBD, PSP	(p83),(p84),(p105),(p106),(p107),(p108),(p109),(p110),(p111),(p112)
L095 (Pinacyanol)	NFTs, NPTs	Not specified	AD	(p113)

N368–F378). In particular, β1 (N-terminal side) includes the PHF6 segment (residues V306–K311), which is known to be involved in the initiation of tau aggregation,[p78] packing with β8 (residues T373–F378). This latter β-strand (residues T373–F378) is also involved in interactions with β2 (residues V313 and C322). The β3 strand (residues N327–K331) is placed in front of β7 (residues S356–V363), whereas β4 (residues V337–S341), β5 (residues K343–K347) and β6 (residues R349–I354) are responsible for the C-shape motif. According to cryo-EM experiments,[p63] the interface between the protofilaments of PHFs extracted from post-mortem brains of AD patients is characterized by a series of van der Waals and H-bond interactions occurring between residues K331–Q336.[p63] The relevance of these residues and their interactions has been recently studied through extensive molecular dynamics simulations.[p13] Moreover, very recently time-resolved cryogenic electron microscopy performed by Lövestam and colleagues further confirmed experimentally that the P332–G335 motif, together with P364–367G, plays a prominent part in the maturation toward C-shaped protofilaments of PHFs in AD.[p66] Besides, SFs are also present in the brain of individuals with AD. These aggregates, which share a core with the same eight β-strand organization and a similar C-shaped protofilament structure of PHFs, are less common in AD, and present a straighter, less-twisted morphology. In particular, SFs are composed of two protofilaments placed in an asymmetric manner. Such a different configuration allows SFs to form a different inter-protofilament interface, which is stabilized only by a series of van der Waals interactions.[p63]

Under pathological conditions, tau can undergo a series of genetic and post-translational modifications (PTMs), some of which can influence the structural diversity of tauopathy strains.[p69] An example in this respect comes from a study reported in 2020 by Arakhamia *et al.*,[p79] the researchers found that ubiquitination can influence tau's inter-protofilament interfaces. This has a direct effect on the polymorph, which can be responsible for the structural and morphological differences in CBD and AD tau filaments. In this respect, several imaging probes detecting tau aggregates in biological fluids or directly in living patients have been developed. In particular, the ones based on PET are the most investigated so far, also in consideration of the relatively low invasiveness of this technique. These probes are designed to bind to tau aggregates in the brain, with the aim of assessing a specific tauopathy in living patients. So far, several PET tracers have been developed (Table 2, Table 3, Figure 3). [^{18}F]Flortaucipir (i.e., [^{18}F]AV-1451, [^{18}F]T-807) and [^{18}F]Florzolotau represent the first tau-specific PET tracers approved by the FDA for clinical use,[p80],[p81],[p82],[p83],[p84],[p85],[p86],[p87],[p88],[p89],[p90],[p91],[p92],[p93],[p94], [p95],[p96],[p97],[p98],[p99],[p100],[p101],[p102],[p103],[p104],[p105],[p106],[p107], [p108], [p109],[p110],[p111],[p112],[p113],[p114], [p115],[p116],[p117],

TABLE 3

***K*d, plasma and physical half-life and main clearance pathway of relevant tau PET probes reported in the literature**

Compound ID	K_d	Half-life	Clearance pathway	Refs
[^{11}C]PBB3	Not available	Physical: 20.4 min	Not available	(p114)
[^{18}F]Flortaucipir (i.e., [^{18}F]AV-1451, [^{18}F]-T807, Tauvid)	0.57 nM PHF in AD	Plasma: 17.0 ± 4.2 min	Renal (kidney excretion)	(p115),(p116)
[^{18}F]T-808	Not available	Physical: 109.8 min	Hepatobiliary system	(p117)
[^{11}C]RO-643 (i.e., [^{11}C]RO-6924963)	Not available	Physical: 20.4 min	Brain	(p89),(p118)
[^{18}F]/[^{3}H]RO-948 (i.e., [^{18}F]/[^{3}H]-RO-6958948)	Not available	Physical: 109.8 min ([^{18}F]RO-948)	Not available	(p119)
[^{11}C]RO-963 (i.e., [^{11}C]RO-6931643)	Not available	Physical: 20.4 min	Not available	(p118)
[^{18}F]Florzolotau (i.e., [^{18}F]PM-PBB3, [^{18}F]APN-1607)	Not available	Physical: 109.8 min Plasma: 16.4 ± 5.4 h	Renal (kidney excretion)	(p120)
[^{18}F]GTP-1	Not available	Physical: 109.8 min	Not available	–
[^{18}F]JNJ-067 (i.e., [^{18}F]JNJ-64326067-AAA)	Not available	Physical: 109.8 min	Not available	–
[^{18}F]JNJ-311	Not available	Physical: 109.8 min	Not available	–
[^{18}F]SNFT-1	Not available	Physical: 109.8 min	Not available	–
[^{18}F]/[^{3}H]MK-6240	0.16 nM for NFTs *in vitro* ([^{3}H]MK-6240)	Physical: 109.8 min ([^{18}F]MK-6240)	Not available	(p86)
[^{18}F]/[^{3}H]PI-2620	Not available	Physical: 109.8 min ([^{18}F]MK-6240)	Not available	–
[^{18}F]S-16	Not available	Physical: 109.8 min ([^{18}F]MK-6240)	Not available	–
[^{18}F]CBD-2115/[^{3}H]CBD-2115	[^{3}H]CBD-2115: 6.9 nM for 4R-tau aggregates (transgenic mouse tissue), 4.9 nM PSP-specific 4R-tau deposits (human brain tissue homogenates)	Physical: 109.8 min ([^{18}F]CBD-2115)	Not available	(p104)
THK compounds ([^{18}F]THK-523, [^{18}F]THK-5105, [^{18}F] THK-5116, [^{18}F]THK-5117 and [^{18}F]]/[^{3}H]THK-5351)	[^{18}F]THK-523: 87 nM [^{18}F]THK-5105: 2.6 nM [^{18}F]THK-5117: 5 nM (AD NFTs *in vitro*)	Physical: 109.8 min ([^{18}F]compounds)	Not available	(p121)
L095 (Pinacyanol)	Not available	Not available	Not available	–

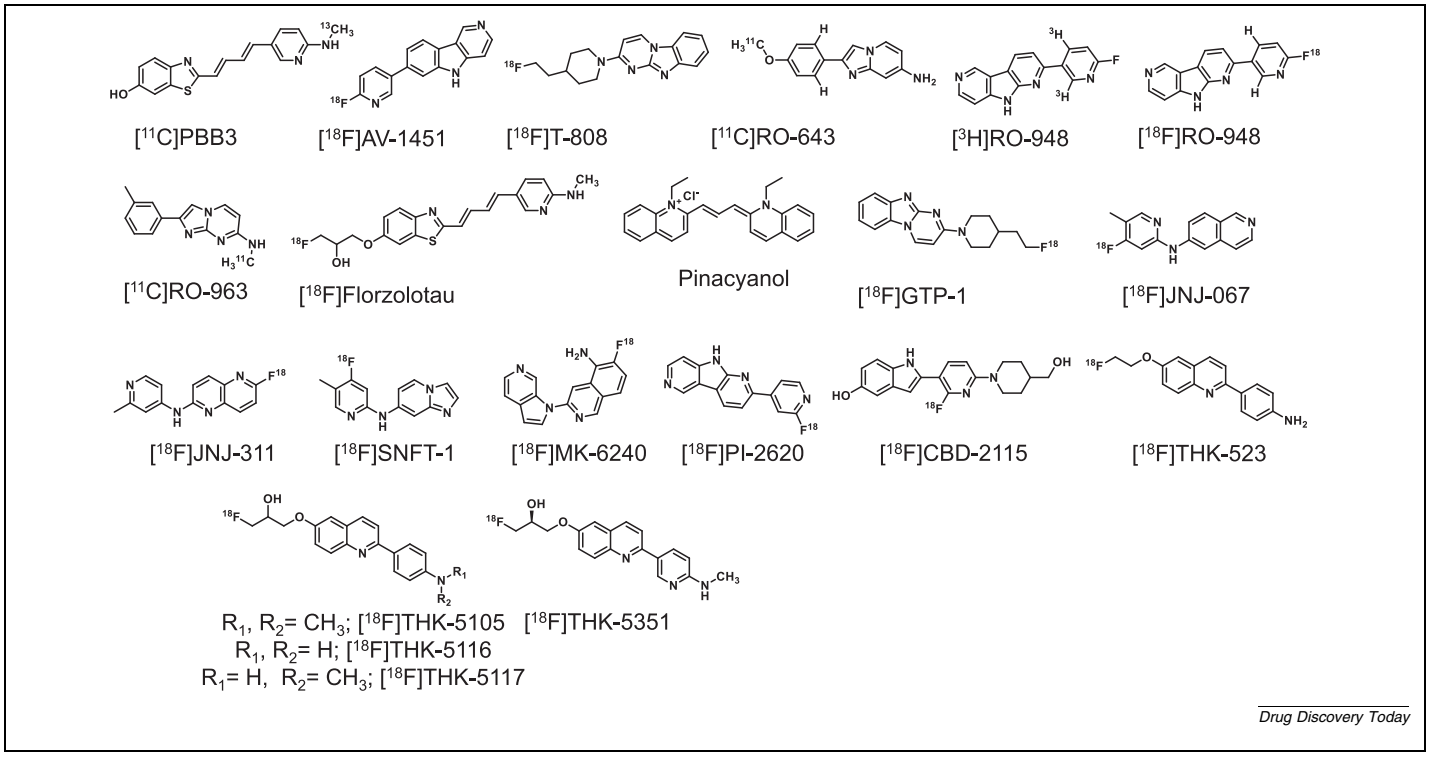

FIGURE 3

Chemical structures of the main tau PET probes reported in literature, the compounds are described in Table 2 and Table 3.

(p118),(p119), (p120),(p121) and the first PET probes to be co-solved in complex with PHFs and SFs, respectively, in cryo-EM experiments (i.e., PDB code: 7NRQ).(p63)

[18F]Flortaucipir is one of the first-generation PET tracers studied for detecting tau aggregates, which binds 3R- and 4R-tau in AD, and to a lesser extent in PSP and CBD aggregates as shown *in vitro* and *in vivo*.(p122) The favorable toxicity profile of [18F]Flortaucipir, combined with its (i) ability to cross the blood–brain barrier; (ii) ability to detect NFTs in good correlation with NFT Braak staging and tau pathology at autopsy(p123) and (iii) selectivity toward aggregates of tau compared with those from other neurodegenerative-related proteins, made this compound a prime player in several research studies and clinical settings.(p124) However, according to several studies, [18F]Flortaucipir also showed off-target interactions. In particular, it displayed binding to neuromelanin- and melanin-containing cells and was demonstrated to accumulate in the basal ganglia, choroid plexus and midbrain regions, which are not generally susceptible to the accumulation of tau aggregates.(p125),(p126) Whereas *in vitro* studies have shown that [18F]Flortaucipir can bind to monoamine oxidase A (MAO-A), studies conducted on *ex vivo* samples have not highlighted significant binding to this enzyme.(p127) To elucidate the mechanism of interaction of this compound and others (e.g., [18F]Florzolotau, GTP-1 and MK-6240) with tau aggregates, thus improving its binding and selectivity properties for tau aggregates in different tauopathies, *in silico* and *in vitro* studies have been performed.(p128),(p129),(p130),(p131)

Although no X-Ray or cryo-EM structure of AD-relevant PHFs in complex with [18F]Flortaucipir have been solved, indications related to a putative binding mode for this compound have been identified,(p61) which corresponded to those of GTP-1 and MK-6240 (Figure 4).(p85),(p86),(p132) The binding mode of GTP-1 (PDB code: 8FUG) and MK-6240 (PDB code: 8UQ7) to AD PHFs has been elucidated by means of cryo-EM experiments (Figure 4).(p92) Interestingly, these two probes shared the same region of interaction of [18F]Florzolotau. According to cryo-EM studies, MK-6240 and GTP-1 bind to the C-shape of AD PHFs in a flat stacking fashion, interacting with residues Q351, K353 and I360. Interestingly, cryo-EM experiments of a chronic traumatic encephalopathy-driven structure resembling the AD PHFs showed that [18F]Flortaucipir binds to the same C-shape site (i.e., PDB code: 8BYN).(p61) To some extent, this is in line with results reported by Bohórquez and colleagues,(p132) by Malarte *et al.*(p85) and Hostetler *et al.*,(p86) which highlighted competitive binding of Flortaucipir and GTP-1 through radiographic *in vitro* competition assays, and of Flortaucipir compared to [3H]MK-6240 through radioligand competition binding experiments on temporal cortex homogenates from cognitively normal and AD human brain donors, respectively. Although these compounds bind to the same site of tau PHFs, they showed different imaging results *in vivo*. For example, [18F]Flortaucipir shows increased accumulations in the medial temporal lobe, neocortical regions and in other areas known to be involved in AD tau pathology,(p133) as well as to correlate with Braak staging.(p124),(p134) However, PET imaging assays revealed accumulation of this compound in the basal ganglia, choroid plexus and substantia nigra owing to interaction with MO-A and other proteins.(p126),(p135),(p136) This compound also binds PSP and CBD tau aggregates *in vitro*.(p124) Notably, GPT-1 shows high affinity for aggregated tau;(p94) this compound has low affinity toward other

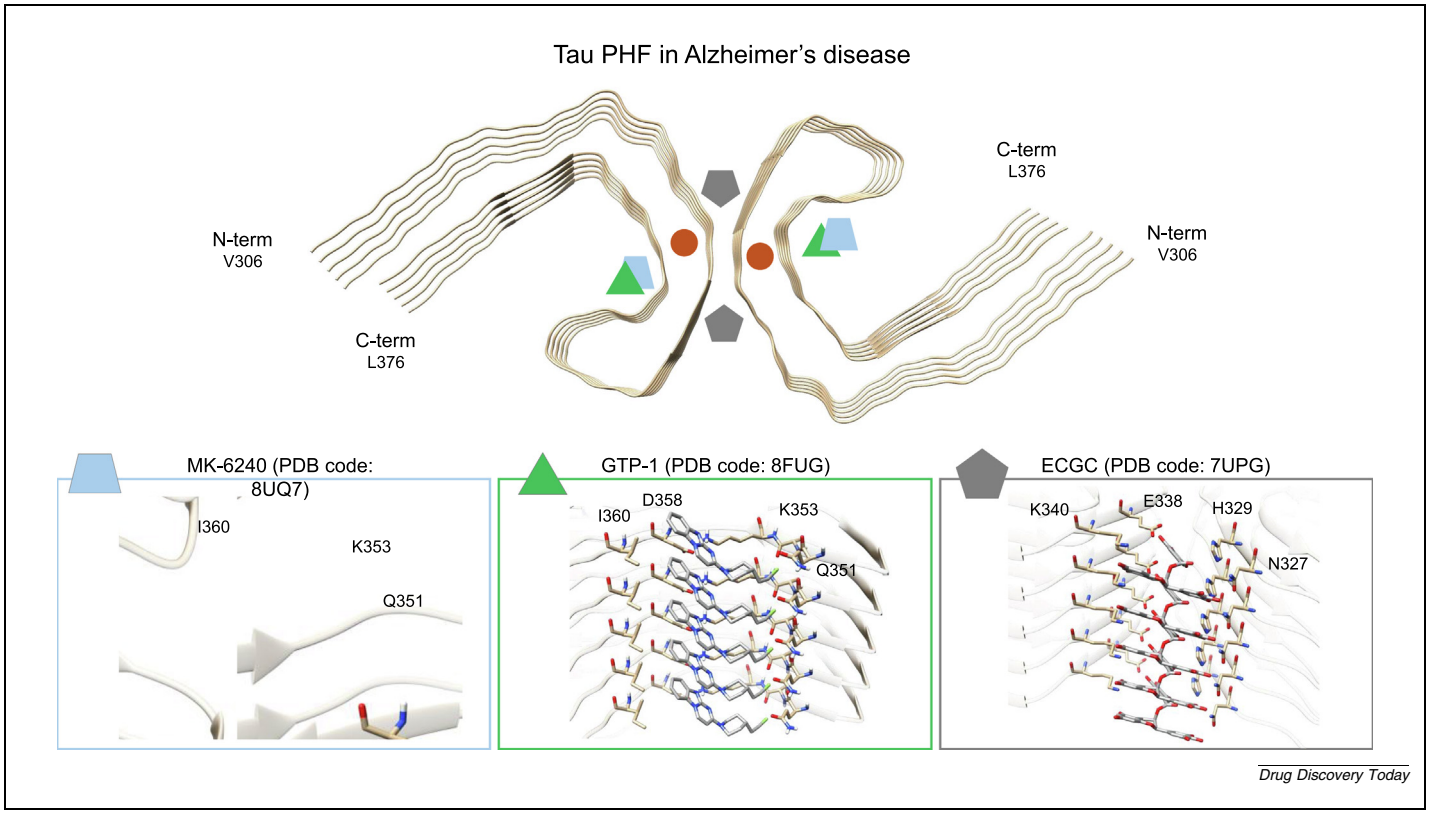

FIGURE 4

Binding sites of MK-6240 (light blue trapezium), GTP-1 (green triangle) and EGCG (light grey pentagon) in the structure of the PHF dimer (PDB ID: 5O3L).[p92] For each ligand, close-up views in the respective binding regions are also reported. The cryptic pockets identified by Rastelli *et al.* are marked by the dark orange circles.[p13] (For interpretation of the references to colour in this figure legend, the reader is referred to the web version of this article.)

aggregation-prone proteins and accumulates more selectively in regions interested in tau inclusions in AD, while there is low-to-no accumulation in bone.[p132] However, these findings need to be validated in larger patient cohorts. MK-6240 was shown to accumulate into bone and meninges, besides AD relevant regions such as the medial temporal lobe[p133] and neocortex.[p137] One of the main factors causing this accumulation could be due to defluorination, which is a common characteristic of [^{18}F] probes.[p86]

Although binding to a broader range of tau isoforms (3R and 4R tau),[p138] [^{18}F]Florzolotau was demonstrated to help detecting tau accumulation in disease-specific regions, and allowed Tagai and co-workers to establish an optimal method for defining reference tissues on PET images of AD and non-AD tauopathy brains, from 40 age-matched healthy controls and 23 with AD, 40 with PSP and five other tau-positive FTLD patients.[p93] This evidence suggests that further studies are needed to elucidate selectivity determinants among the various tau polymorphs. Recently, additional sites of interaction have been elucidated in tau PHF cryo-EM structures. One example comes from the structure of tau PHFs binding to EGCG, recently reported by Seidler *et al.* (Figure 4).[p139] In this structure, EGCG binds to a different region of tau PHFs, in a site lined by the junction of two tau protofilaments. In this cleft, EGCG binds with diagonal stacking fashion, making polar contacts and H-bonds with N327, H329, E338 and K340, and adopting a planar conformation stabilized by a series of intramolecular π-π interactions (Figure 4).[p139] Cryo-EM experiments demonstrated that compounds binding to tau such as MK-6240, GTP-1 and EGCG perform peculiar ligand–PHF interactions (Figure 4),[p140] suggesting structural insights on the binding mode that might be exploited for the design of novel tau ligands.[p92] These findings also fueled the research toward the application of *in silico* structure-based approaches to design novel tau PHF binding compounds.[p141] These *in silico* investigations[p13] highlighted PHF cryptic sites, which might be exploited for the design of novel tracers. Indeed, future efforts will help to better assess the relevance of these experimentally derived binding modes and *in silico* data for the design of more-selective tau PET tracers.[p140],[p142]

Pick's disease

Falcon *et al.* showed that PiD core filaments consist of residues K254–F378 of 3R-tau, which are folded differently to AD PHFs and SFs.[p49] This suggests the existence of polymorphs in different tauopathies. The two main populations consist of narrow and wide filaments (NPFs and WPFs, respectively), with the first type accounting for 93% of the overall filament population. One of the main structural differences relies on the filament width, which varies from 50 Å (NPFs) to 300 Å (WPFs). Notably, NPFs are composed of a single protofilament markedly different from the C-shaped protofilament of AD filaments.[p49] The NPF core is composed of nine β-strands (β1–9) arranged into four cross-β

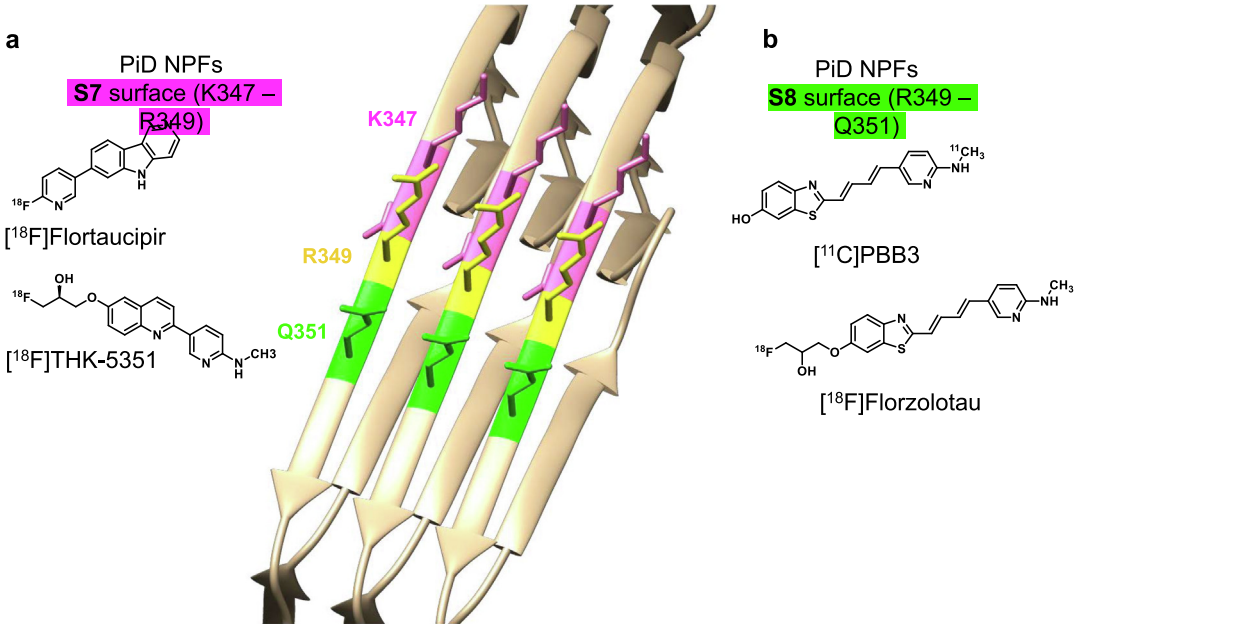

FIGURE 5

In PiD NFs, the interaction surfaces S7 and S8 (both provided by the β-strand β7) bind with different affinity to various PET imaging probes. **(a)** The structure of the probes binding with the highest affinity to S7 are depicted. **(b)** The structure of the two tracers mainly involved in S8 interaction are provided. Residue R349, common to surfaces S7 and S8, is depicted in yellow. RCSB PDB file: 6GX5.[p49] (For interpretation of the references to colour in this figure legend, the reader is referred to the web version of this article.)

packing stacks. The MBR segment R1 provides the strands β1 and β2, whereas R3 is responsible for β3–5 and R4 for β6–8. The final strand, β9, is made of nine amino acids after R4 and packs against the opposite side of β8. Notably, WPFs are formed by two separate protofilaments making tight contacts at their distal tips through van der Waals interactions. Unlike AD PHFs and SFs, PiD filaments are not phosphorylated at S262 and/or S356. This suggests that different folds are responsible for tauopathies with 4R-tau filaments, like PSP. These data raised the question as to whether different tau filament structures can be distinguished by molecular probes, some of which were developed for *in vivo* PET imaging.[p143] Lately, several tau tracers: [^{11}C]PBB3, [^{18}F]Florzolotau, [^{18}F]Flortaucipir, [^{18}F]THK-5351, [^{18}F]MK-6240, [^{18}F]RO-6958948, [^{18}F]GTP-1 and [^{18}F]PI-2620, were developed for human imaging, with different pharmacokinetics profiles and selectivity.[p21],[p51],[p91],[p93],[p135],[p143],[p144],[p145]

As depicted from Falcon *et al.*, PiD filaments fold in a J-shaped structure, instead of the C shape seen in patients with AD.[p49] Mishra *et al.* conducted modeling studies that identified the inner cavity C1 formed between P312-V313-D314 and P332-G333-G334 as the hottest spot for PET probes binding.[p143] Notably, rescoring energies predict [^{13}C]PBB3 to be the most potent binder for the interaction surface S7, which is part of the strand β7 provided by tau MBR R4 according to Falcon *et al.* (Figure 2).[p49],[p143] These studies, which did not take into account protein flexibility and solvent effects, were validated by molecular dynamics simulations. In particular, MM/GBSA-binding free energy calculations predicted the interaction surface S7 as the most potent for Flortaucipir and [^{18}F]THK-5351, and S8 for [^{13}C]PBB3 and [^{18}F]Florzolotau (Figure 5). These studies suggest that [^{13}C]PBB3, previously used to visualize tau deposition in AD and PiD, shows binding to multiple surface sites, with S7 and S8 having the strongest binding free energy values (−27.6 kcal/mol and −27.9 kcal/mol, respectively). Surprisingly, the fluorinated derivative [^{18}F]Florzolotau shows a high affinity for S8 compared to PBB3. Thus, [^{13}C]PBB3 and [^{18}F]Florzolotau were confirmed to be potent traces for PiD, as suggested from previous preclinical and clinical data. Whereas [^{13}C]PBB3 shows a good binding affinity for tau deposits in AD and PiD, [^{18}F]Florzolotau seems to be more selective for PiD. This is consistent with its unique binding feature, because it interacts tightly with the surface S8, one of the two characteristic surfaces together with S7 of PiD.[p143] As shown in other studies, [^{18}F]Florzolotau is also used for PET imaging of other models of tauopathies, in particular in frontotemporal dementia (FTD)-related diseases.[p146],[p147] Although this tracer can be a good starting point for the obtainment of PiD tracers, more efforts are required from researchers to develop selective, potent imaging probes to discriminate among different tauopathies.

Progressive supranuclear palsy

Tau filaments in PSP are made of a single protofilament with an ordered core spanning residues 272–381, corresponding to the last residue of R1, the repeats R2–R4, and a part of the C-terminal domain.[p1] Although they share the same core residues of tauopathies, similarly to CBD, they adopt a different and peculiar folding. In particular, R2, R3 and R4 form a three-layer structure with turns located at the conserved PGGG motifs at the end

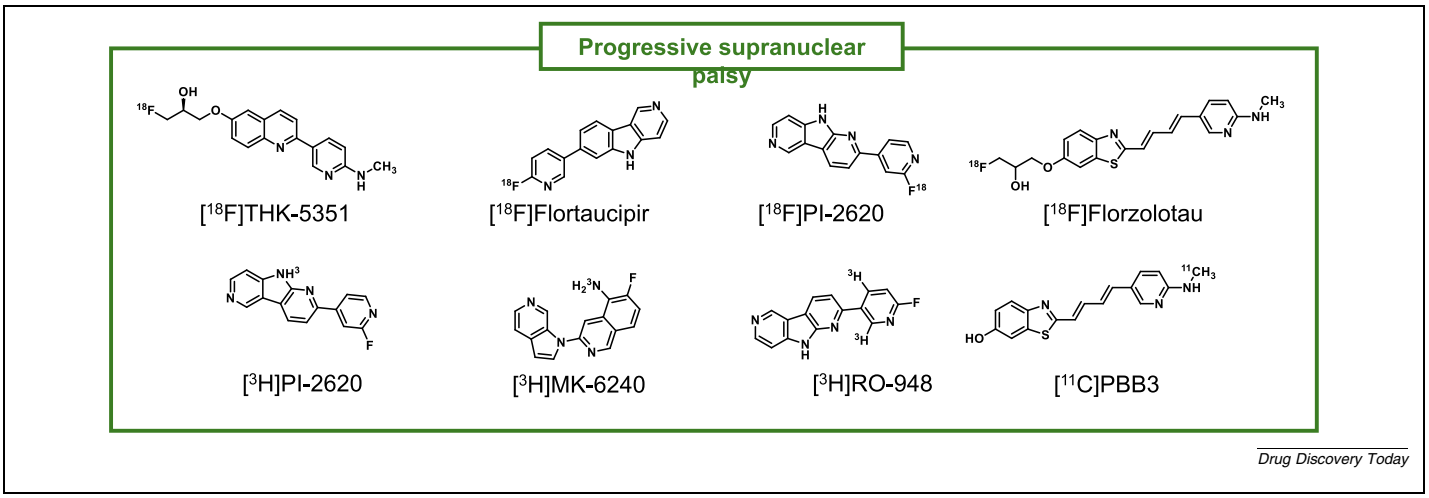

FIGURE 6
The chemical structures of the main probes proposed for PSP detection are shown.

of each repeat (residues 301–304 for R2, 332–335 for R3, 334–337 for R4).[p1] Shi *et al.* showed that the central layer is formed by R3, with R2 packed against this repeat. Of note, the R2–R3 interface contains two cavities. The one between N279 and G323 is surrounded by hydrophobic side chains, whereas the other next to the salt bridge is likely to be a solvent molecule.[p1] At the R3–R4 interface, there is a cavity between the positively charged K317, K321 and K340 allocating anionic molecules. The rest of the R3–R4 interface involves hydrophobic interactions and a salt bridge between K311 and D348.[p1] These filaments are found in NFTs, a common feature in tauopathies like PSP, AD, PiD and CBD. However, these inclusions are distinct between AD and PSP, because they differ in the localization and type of tau isoforms.[p64] In PSP, tau inclusions are also present in tuft-shaped astrocytes (TAs), which are not found in AD and represent another histopathological hallmark of this pathology.[p64]

Other differences among tau pathologies are based on the protein post-translational modifications. Ebashi *et al.* reported that N279 of 4R-tau is deamidated to aspartic acid in AD postmortem brains, whereas this phenomenon is not present in PSP.[p64] In particular, this post-translational modification is not enzyme-mediated. Indeed, imaging or immune-responsive probes that can detect PSP-specific post-translational changes might provide a valuable strategy to discriminate PSP-type lesions from other tauopathy lesions in the brain or within a single neuron at the molecular level (Figure 6). Recently, Brendel *et al.* showed that the PET probe [^{18}F]THK-5351 had an enhanced *in vivo* uptake in the midbrain, thus discriminating PSP patients from age-matched controls.[p145] Notably, in the PSP-diagnosed group, the mean [^{18}F]THK-5351 PET signal was significantly elevated in the midbrain, bilateral globus pallidus, bilateral frontal cortex and medulla oblongata.[p145] This peculiar distribution matched the tau inclusions localization found in the postmortem histological samples.[p145] These data demonstrate that the probe [^{18}F]THK-5351 was able to discriminate PSP patients from controls even at earlier disease stages. However, these findings need to be validated in a larger patient cohort. Also, further experiments need to address which fraction of [^{18}F]THK-5351 binds selectively to patient tau deposits and which one is related to MAO-B binding, a potential off-target of PET probes. Indeed, MAO-B is widely distributed in the brain, being particularly present in astrocytes. Therefore, this off-target binding could worsen the quality of tau inclusion detection. Even if promising, it has been confirmed that [^{18}F]THK-5351 is not suitable as a PET tracer for evaluating tau accumulation in PSP at present.[112] Another interesting ligand in this field is [^{18}F]Flortaucipir, which proved to distinguish PSP from PD and AD patients *in vivo*.[p145] However, the selectivity of this tracer toward tau PSP inclusions is ambiguous, because *ex vivo* PSP autoradiography studies showed no binding of [^{18}F]Flortaucipir to these aggregates.[p90] Indeed, more studies need to be carried out to characterize the binding specificity of this probe. In particular, age-matched controls have to be included to validate the selectivity of [^{18}F]Flortaucipir toward tau inclusions in PSP patient brains.

[^{18}F]PI-2620, [^{3}H]MK-6240, [^{3}H]PI-2620 and [^{3}H]RO-948 also emerged as interesting PET probes for tauopathy imaging, in particular for PSP.[p90] [^{18}F]PI-2620 was shown to recognize tau inclusions in AD, CBD and PSP brains, compared with age-matched controls. Interestingly, the binding pattern observed in PSP and CBD was different than the one seen in AD.[p90] By contrast, no *in vitro* binding of [^{3}H]MK-6240, [^{3}H]PI-2620 and [^{3}H]RO-948 could be observed using autoradiography in the PSP frontal cortex. However, the probe [^{3}H]PI-2620 was able to bind tau deposits with high affinity in the CBD brain, probably because of two binding sites present on the target surfaces.[p90] In this regard, it is also worth mentioning that [^{11}C]PBB3 and [^{18}F]Florzolotau are able to bind to tau lesions in PSP, in clinical and in post-mortem brains, according to an unbiased, automated diagnostic method.[p148]

Corticobasal degeneration

Similarly to PSP, CBD tau filaments are composed of a common protofilament whose core spans residues K274–E380 and folds in 11 β-sheets.[p53] These secondary structure elements are connected by turns and arcs to form a four-layered structure. In particular, the central layers are formed by β7, β4, β3 and β10, whereas β2, β5 and β6 form a three-layered structure on the other

side. A hydrophobic cavity is formed by residues from β2, β3, β10, β11 and the connections between β1 and β2. Interestingly, the other interfaces constituting CBD tau filaments have mixed compositions of polar and hydrophobic groups.[p53] The structural similarity to PSP filaments has made the selective identification of these two tauopathies particularly challenging. Of note, both are 4R tauopathies, thus sharing the same tau isoforms. Furthermore, tau isoform 4R is also present in AD inclusions, thus blurring the distinction of these neurodegenerative disorders. Notwithstanding, the different folding, post-translational modifications and local dissimilarities in the filament core have been exploited to selectively recognize these pathologies. In this field, imaging probes that can detect characteristic features could represent an interesting solution (Figure 7).

For example, PET studies with [^{18}F]PI-6240, [^{18}F]MK-6240 and [^{18}F]Florzolotau have been reported in the literature for the molecular imaging of AD, PSP and CBD patients. Data showed that [^{18}F]MK-6240 had no significant binding in PSP and CBD cases, thus it was able to discriminate AD from other tauopathies through selective binding to AD tau inclusions.[p129] In this field, Zhou *et al.* showed by computational simulations that different tau tracers demonstrated preferences for distinct binding sites on the same CBD tau filament.[p129] [^{18}F]PI-2620 showed the strongest binding affinity to CBD-tau at the concave site s12 – a hydrophobic pocket between strands β2 and β5 (Figure 8). Interestingly, this site was not favorable for the binding of [^{18}F]CBD-2115, another tracer developed to selectively distinguish 4R tauopathies. The latter compound demonstrated a stronger binding affinity to the entry site e1 (between K281 of β1 and L376 of β11) and the core site c1 (hydrophobic region composed of V306, V339 and L344, between β4 and β7), as shown in Figure 8. This peculiar entry side e1 was also targeted with high affinity by the tracer [^{18}F]Florzolotau and [^{18}F]PI-6240 (Figure 8). In particular, the PET probe [^{18}F]PI-6240 forms stable interaction with residues N279 and K281 of the above-mentioned interacting site. Above all, [^{18}F]MK-6240 showed the lowest affinity for CBD filaments. Although some PET tracers displayed a good affinity and selectivity for CBD inclusions, none of them was able to discriminate with high accuracy between the different tau pathologies.

Of note, CBD-2115, which was experimentally designed to bind to tau 4R inclusions, presented low *in vivo* uptake and high staining of AD samples. Therefore, selectivity remains an issue that needs to be addressed by the next-generation tracers. In this regard, recent PET scans and brain biopsies showed that [^{11}C]PBB3 was able to bind CBD-type tau inclusions in the brains of living individuals.[p149] At the same time, Flortaucipir was reported to detect tau depositions in CBD brains in the motor cortex and adjacent areas in distinction from AD and PSP subjects.[p149] Although these results are promising and move toward the direction of a potent and selective CBD tracer, the study of Nakano *et al.* has some limitations to be addressed. First, the authors have to validate their data on a larger sample size. Then, the parameters of healthy-control reference tissue need optimization, to ameliorate the robustness of the study results.[p149]

Concluding remarks and future perspectives

This review highlights the recent advances and challenges in developing imaging probes to selectively detect polymorphic tau aggregates across major tauopathies, including AD, PiD, PSP and CBD. The detection of tau polymorphs specific to each pathology holds great potential for improving diagnostic accuracy and early intervention, yet current technologies exhibit limitations in sensitivity, selectivity and clinical applicability.[p69],[p150],[p151],[p152] Although different tauopathies are characterized by distinct tau polymorphs, at present no single probe offers the precision necessary to unambiguously identify these polymorphs in a clinical setting. For example, the cryo-

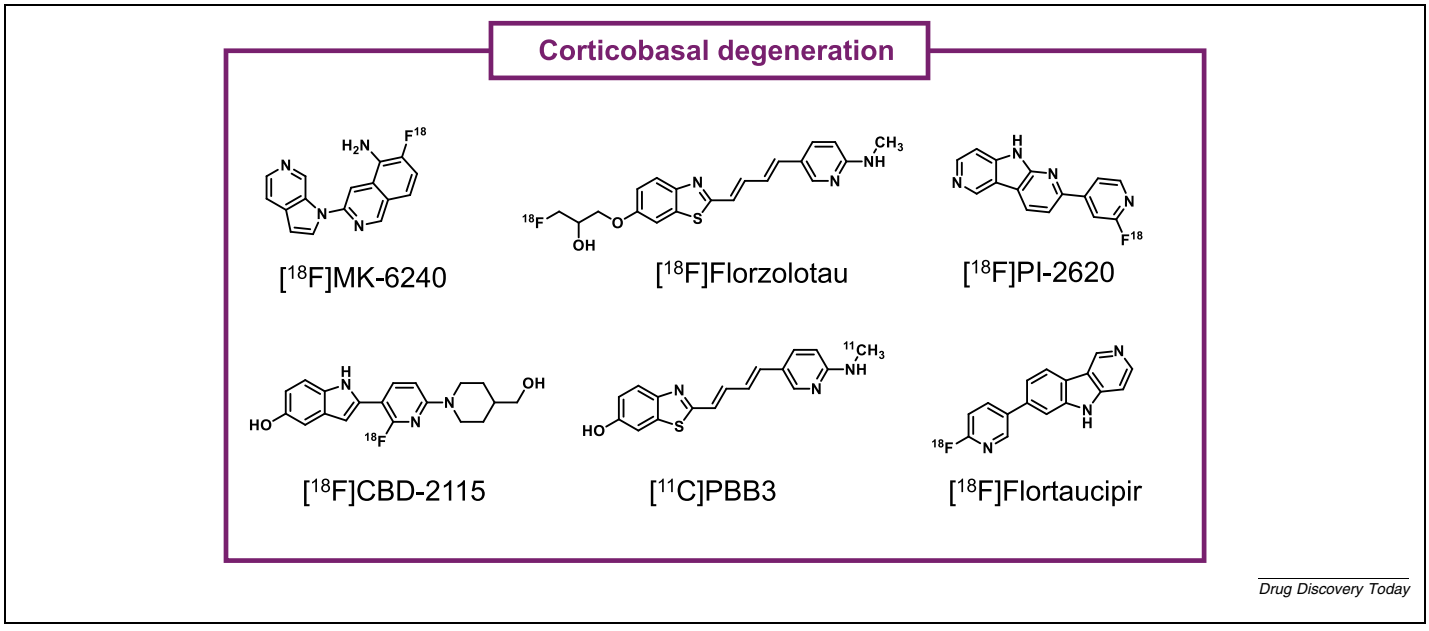

FIGURE 7
The structures of the imaging probes studied for the detection of CBD are reported.

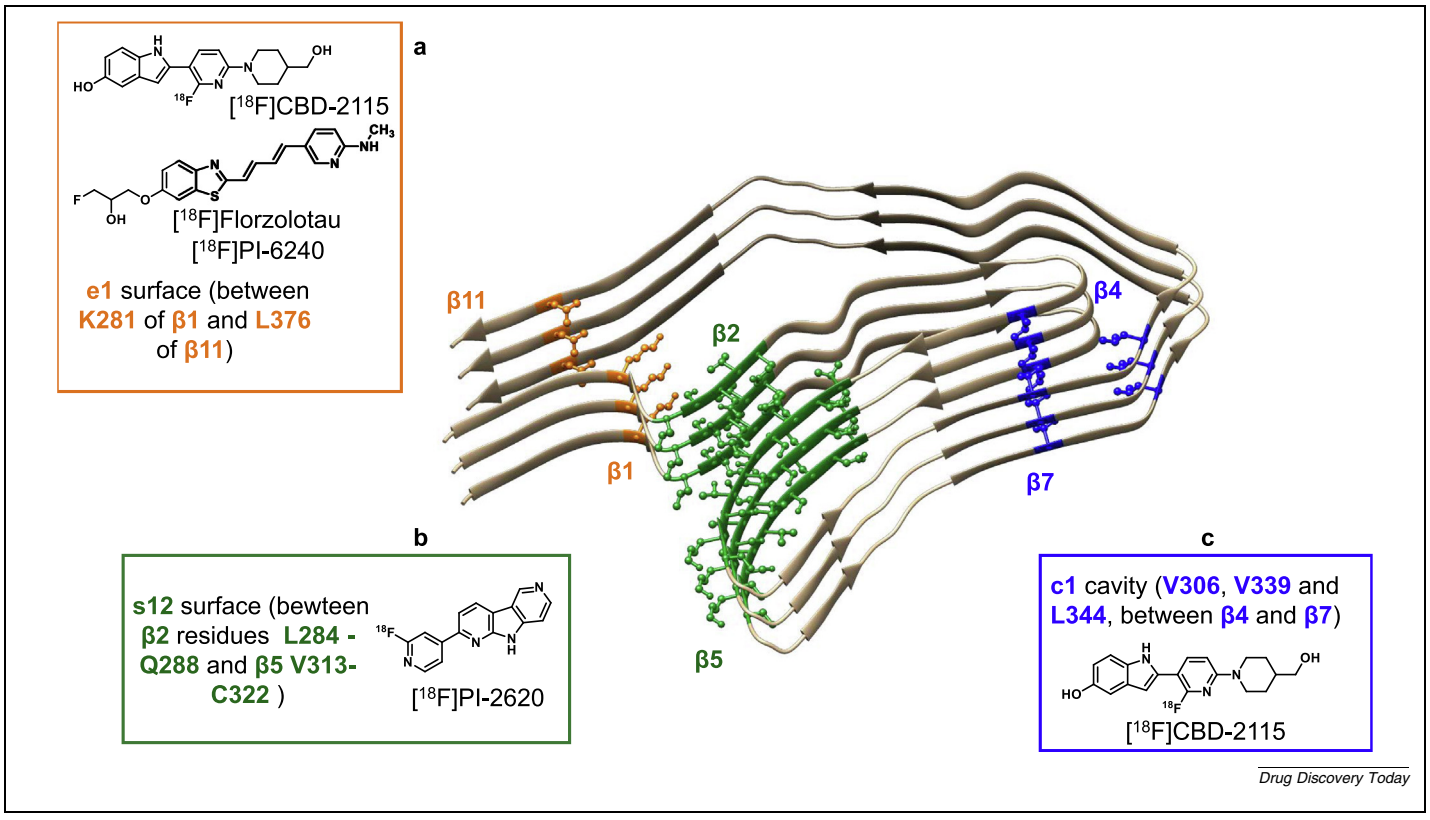

FIGURE 8

In CBD filaments, the interaction surfaces s12, the sites e1 and the cavity c1 are involved in the interaction with various PET imaging probes (PDB file: 6VHA). **(a)** The structure of the probes binding with the highest affinity to s12 are depicted. **(b)** The PET imaging tracers able to bind to the e1 surface are represented (the structure of [^{18}F]PI-6240 is not provided). **(c)** The probe [^{18}F]CBD-2115 binds with high affinity to the c1 cavity, embedded between β4 and β7.

EM work on PiD identified unique J-shaped tau NPFs, which are markedly different from the C-shaped PHFs and SFs found in AD.[(p45),(p49)] PET tracers such as [^{18}F]Florzolotau become relevant in this context, being selective for the specific structural folds of PiD tau inclusions at binding surfaces S7 and S8.[(p146)] However, additional work is required to validate selectivity across larger patient cohorts and to improve the accuracy of early detection in clinical settings.

Similarly, PSP and CBD present distinct tau filament folds that are difficult to distinguish, owing to overlapping tau isoforms and core regions. However, PSP (characterized by tau filament core 272–381) lacks post-transcriptional modifications like N279 deamidation, which is present in AD filaments.[(p153)] Although PET tracers such as [^{18}F]THK-5351 show enhanced binding in PSP-related brain regions, selectivity remains an issue because of potential off-target binding, such as interaction with MAO-B, complicating the tracer's specificity to PSP tau aggregates.[(p145)] Moreover, [^{18}F]Flortaucipir has been shown to detect tau aggregates in PSP but failed in differentiating PSP lesions from AD inclusions, highlighting the need for improved probes with reduced off-target effects and enhanced disease-specific binding profiles.[(p135),(p154)] In CBD, tau filaments share structural similarities with PSP filaments but exhibit a unique concave binding pocket at site s12, which could provide a basis for probe selectivity.[(p129)] Tracers like [^{18}F]PI-2620 have demonstrated binding to tau inclusions in CBD pathology, although their selectivity across tauopathies remains under evaluation. Notably, the probes GTP-1 and MK-6240 showed great potential in selectively binding to AD inclusions but results must be confirmed in larger patient cohorts. Instead, promising probes like [^{18}F]Florzolotau and [^{18}F]Florzolotau also exhibited affinity for other tauopathies like CBD and PSP.[(p132),(p137),(p142)]

One straightforward approach to improve compound selectivity toward disease-specific tau polymorphs features could be structure-based drug design (SBDD). By utilizing structural insights from cryo-EM and computational modeling, researchers can design or optimize probes that specifically target disease-specific tau conformations. This opportunity is made possible by the ever-increasing resolution of cryo-EM structures of tau.[(p22)] By focusing on unique binding sites, such as the S7 and S8 surfaces in PiD[(p143)] or the hydrophobic site s12 in CBD,[(p129)] new probes can be designed that selectively interact with tau polymorphs specific to each disease.

Owing to advanced organic chemistry techniques, the core of the probes that bind to these interaction surfaces could be joined together to create additional anchoring points. This would ideally lead to compounds bearing a stronger binding affinity and increased selectivity for specific surfaces or cavities found on tau polymorphs. This approach can also involve designing molecules based on post-translational modifications, such as deamidation patterns unique to AD tau inclusions, as potential selective binding sites.[(p64)] SBDD was successfully applied for the identification of tau aggregation inhibitors, like the antibody PNT001[(p155),(p156)] and the small molecules Anle138b[(p157),(p158)]

and PHOX15.[p13] More importantly, SBDD exploitation led to the probe [^{18}F]Flortaucipir (designed on AD PHFs), one of the gold standards for tau PET imaging, which unfortunately bears off-target binding to other tauopathies.[p71],[p159] Again, the combination of molecular dynamics simulations and fragment-based design for tau-specific binding pockets was crucial for the discovery of MK-6240 and THK-5351.[p21],[p90],[p145],[p160] The combination of experimental (cryo-EM) and computational (molecular dynamics and docking) investigations performed on different tau polymorphs could shed additional light on how to turn tau-binding scaffolds into selective compounds.

Another useful approach to increase selectivity is to design *ad hoc* chemical modifications to already known probes. Selectivity can be tuned by modifying core structures or functional groups to enhance affinity for unique tau polymorphs. For example, fluorinated derivatives like [^{18}F]Florzolotau show increased selectivity for PiD tau inclusions over other tauopathies,[p143] a principle that could be applied to other classes of probes. In this context, SAR and structure–selectivity relationships (SSR) could be extremely useful. Such relationships could be built by leveraging the large amounts of data reported in databases as ChEMBL,[p161] Protein Data Bank (PDB),[p162] BindingDB,[p163], and Molecular Imaging and Contrast Agent Database (MICAD).[p164] These SAR and SSR would greatly help to understand which modifications might increase binding and selectivity.

Finally, probes that can advance to clinical applications must demonstrate low toxicity and suitable pharmacokinetics. Therefore, efforts should continue to optimize metabolic stability, solubility and brain penetration, particularly for PET tracers. Novel chemotypes, such as those based on thiophene-π systems, could offer safer, more-effective alternatives for *in vivo* applications, owing to deep tissue penetration, minimized biological interference and low toxicity.[p75] With a concerted focus on these medicinal chemistry approaches, future probe development can move closer to realizing highly selective, clinically viable imaging agents for tauopathies.

Author contributions

The manuscript was written through contributions of all authors. All of them have given approval to the final version of the manuscript.

Conflicts of interest

The authors declare that they have no known competing financial interests or personal relationships that could have appeared to influence the work reported in this paper.

Data availability

No data was used for the research described in the article.

Acknowledgments

The authors declare that financial support was received for the research, authorship and/or publication of this article. The research leading to these results has received funding from the European Union – NextGenerationEU through the Italian Ministry of University and Research under PNRR–M4C2-I1.3 Project PE_00000019 “HEAL ITALIA” to GR and NB. The views and opinions expressed are those of the authors only and do not necessarily reflect those of the European Union or the European Commission. Neither the European Union nor the European Commission can be held responsible for them. LP would like to thank the Italian funding program Fondo Sociale Europeo REACT-EU—PON “Ricerca e Innovazione” 2014–2020—Azione IV.4 “Dottorati e contratti di ricerca su tematiche dell’innovazione” for supporting his research.

References

1. Shi Y et al. Structure-based classification of tauopathies. *Nature*. 2021;598:359–363.
2. Arendt T, Stieler JT, Holzer M. Tau and tauopathies. *Brain Res Bull*. 2016;126:238–292.
3. Zhang Y, Wu KM, Yang L, Dong Q, Yu JT. Tauopathies: new perspectives and challenges. *Mol Neurodegener*. 2022;17:28.
4. Bahia VS, Takada LT, Deramecourt V. Neuropathology of frontotemporal lobar degeneration: a review. *Dement Neuropsychol*. 2013;7:19–26.
5. Silva MC, Haggarty SJ. Tauopathies: deciphering disease mechanisms to develop effective therapies. *Int J Mol Sci*. 2020;21:8948.
6. Bakota L, Brandt R. Tau biology and tau-directed therapies for Alzheimer’s disease. *Drugs*. 2016;76:301–313.
7. Khan S, Hassan MI, Shahid M, Islam A. Nature’s toolbox against tau aggregation: an updated review of current research. *Ageing Res Rev*. 2023;87, 101924.
8. Bandyopadhyay B, Li G, Yin H, Kuret J. Tau aggregation and toxicity in a cell culture model of tauopathy. *J Biol Chem*. 2007;282:16454–16464.
9. Fath T, Eidenmüller J, Brandt R. Tau-mediated cytotoxicity in a pseudohyperphosphorylation model of Alzheimer’s disease. *J Neurosci*. 2002;22:9733–9741.
10. Eidenmüller J, Fath T, Hellwig A, Reed J, Sontag E, Brandt R. Structural and functional implications of tau hyperphosphorylation: information from phosphorylation-mimicking mutated tau proteins. *Biochemistry*. 2000;39:13166–13175.
11. Goedert M. The ordered assembly of tau is the gain-of-toxic function that causes human tauopathies. *Alzheimers Dement*. 2016;12:1040–1050.
12. Samudra N, Lane-Donovan C, VandeVrede L, Boxer AL. Tau pathology in neurodegenerative disease: disease mechanisms and therapeutic avenues. *J Clin Invest*. 2023;133, e168553.
13. Pinzi L et al. Quantitative live cell imaging of a tauopathy model enables the identification of a polypharmacological drug candidate that restores physiological microtubule interaction. *Nat Commun*. 2024;15:1679.
14. Liang SY, Wang ZT, Tan L, Yu JT. Tau toxicity in neurodegeneration. *Mol Neurobiol*. 2022;59:3617–3634.
15. Niewiadomska G, Niewiadomski W, Steczkowska M, Gasiorowska A. Tau oligomers neurotoxicity. *Life (Basel)*. 2021;11:28.
16. Ward SM, Himmelstein DS, Lancia JK, Binder LI. Tau oligomers and tau toxicity in neurodegenerative disease. *Biochem Soc Trans*. 2012;40:667–671.
17. Ghag G et al. Soluble tau aggregates, not large fibrils, are the toxic species that display seeding and cross-seeding behavior. *Protein Sci*. 2018;27:1901–1909.
18. Andronesi OC et al. Characterization of Alzheimer’s-like paired helical filaments from the core domain of tau protein using solid-state NMR spectroscopy. *J Am Chem Soc*. 2008;130:5922–5928.
19. Kurihara M et al. CSF P-Tau181 and other biomarkers in patients with neuronal intranuclear inclusion disease. *Neurology*. 2023;100:e1009–e1019.
20. Moloney CM, Lowe VJ, Murray ME. Visualization of neurofibrillary tangle maturity in Alzheimer’s disease: a clinicopathologic perspective for biomarker research. *Alzheimer’s Dementia*. 2021;17:1554–1574.
21. Pascoal TA et al. *In vivo* quantification of neurofibrillary tangles with [18F]MK-6240. *Alzheimers Res Ther*. 2018;10:74.
22. Pinzi L, Bisi N, Sorbi C, Franchini S, Tonali N, Rastelli G. Insights into the structural conformations of the tau protein in different aggregation status. *Molecules*. 2023;28:4544.

23. Kolarova M, García-Sierra F, Bartos A, Ricny J, Ripova D. Structure and pathology of tau protein in Alzheimer disease. *Int J Alzheimers Dis*. 2012;2012, 731526.
24. Stefanoska K et al. An N-terminal motif unique to primate tau enables differential protein–protein interactions. *J Biol Chem*. 2018;293:3710–3719.
25. Derisbourg M et al. Role of the Tau N-terminal region in microtubule stabilization revealed by new endogenous truncated forms. *Sci Rep*. 2015;5:9659.
26. Wang Y, Mandelkow E. Tau in physiology and pathology. *Nat Rev Neurosci*. 2016;17:5–21.
27. Brue CR, Acosta K, Rhoades E. The critical role of the proline rich region (PRR) of tau in physiological microtubule assembly and Alzheimer's disease pathology. *Biophys J*. 2024;123:216a.
28. Dujardin S, Commins C, Lathuiliere A, et al.. Tau molecular diversity contributes to clinical heterogeneity in Alzheimer's disease. *Nat Med*. 2020;26:1256–1263.
29. Kellogg EH, Hejab NMA, Poepsel S, Downing KH, DiMaio F, Nogales E. Near-atomic model of microtubule-tau interactions. *Science*. 2018;360:1242–1246.
30. Ciasson BI et al. Initiation and synergistic fibrillization of tau and alpha-synuclein. *Science*. 2003;300:636–640.
31. Daniele S et al. α-Synuclein aggregated with tau and β-amyloid in human platelets from healthy subjects: correlation with physical exercise. *Front Aging Neurosci*. 2018;10. https://doi.org/10.3389/fnagi.2018.00017.
32. Clinton LK, Blurton-Jones M, Myczek K, Trojanowski JQ, LaFerla FM. Synergistic interactions between Aβ, Tau, and α-synuclein: acceleration of neuropathology and cognitive decline. *J Neurosci*. 2010;30:7281–7289.
33. Lu J et al. Structural basis of the interplay between α-synuclein and Tau in regulating pathological amyloid aggregation. *J Biol Chem*. 2020;295:7470–7480.
34. Irwin DJ, Hurtig HI. The contribution of tau, amyloid-beta and alpha-synuclein pathology to dementia in lewy body disorders. *J Alzheimers Dis Parkinson*. 2018;08. https://doi.org/10.4172/2161-0460.1000444.
35. Moussaud S, Jones DR, Moussaud-Lamodière EL, Delenclos M, Ross OA, McLean PJ. Alpha-synuclein and tau: teammates in neurodegeneration? *Mol Neurodegener*. 2014;9:43.
36. Torres-Garcia L et al. Monitoring the interactions between alpha-synuclein and tau in vitro and in vivo using bimolecular fluorescence complementation. *Sci Rep*. 2022;12:2987.
37. Yan X, Uronen RL, Huttunen HJ. The interaction of α-synuclein and tau: a molecular conspiracy in neurodegeneration? *Semin Cell Dev Biol*. 2020;99:55–64.
38. Akr D, R K, S W, Kh L. Tau interacts with the C-terminal region of α-synuclein, promoting formation of toxic aggregates with distinct molecular conformations. *Biochemistry*. 2019;58:2814–2821.
39. Hanger DP et al. Novel phosphorylation sites in tau from Alzheimer brain support a role for casein kinase 1 in disease pathogenesis. *J Biol Chem*. 2007;282:23645–23654.
40. Rissman RA et al. Caspase-cleavage of tau is an early event in Alzheimer disease tangle pathology. *J Clin Investig*. 2004;114:121.
41. Kim Y et al. Caspase-cleaved tau exhibits rapid memory impairment associated with tau oligomers in a transgenic mouse model. *Neurobiol Dis*. 2016;87:19–28.
42. Gamblin TC et al. Caspase cleavage of tau: linking amyloid and neurofibrillary tangles in Alzheimer's disease. *Proc Natl Acad Sci*. 2003;100:10032–10037.
43. Barbier P et al. Role of tau as a microtubule-associated protein: structural and functional aspects. *Front Aging Neurosci*. 2019;11. https://doi.org/10.3389/fnagi.2019.00204.
44. Jouanne M, Rault S, Voisin-Chiret AS. Tau protein aggregation in Alzheimer's disease: an attractive target for the development of novel therapeutic agents. *Eur J Med Chem*. 2017;139:153–167.
45. Fitzpatrick AWP et al. Cryo-EM structures of tau filaments from Alzheimer's disease. *Nature*. 2017;547:185–190.
46. Falcon B et al. Tau filaments from multiple cases of sporadic and inherited Alzheimer's disease adopt a common fold. *Acta Neuropathol*. 2018;136:699–708.
47. Harrison TM, Maass A, Adams JN, Du R, Baker SL, Jagust WJ. Tau deposition is associated with functional isolation of the hippocampus in aging. *Nat Commun*. 2019;10:4900.
48. Irwin DJ et al. Deep clinical and neuropathological phenotyping of Pick's disease. *Ann Neurol*. 2016;79:272–287.
49. Falcon B et al. Structures of filaments from Pick's disease reveal a novel tau protein fold. *Nature*. 2018;561:137–140.
50. Kovacs GG et al. Distribution patterns of tau pathology in progressive supranuclear palsy. *Acta Neuropathol*. 2020;140:99–119.
51. Martínez-Maldonado A et al. Molecular processing of tau protein in progressive supranuclear palsy: neuronal and glial degeneration. *J Alzheimers Dis*. 2021;79:1517–1531.
52. Kouri N, Whitwell JL, Josephs KA, Rademakers R, Dickson DW. Corticobasal degeneration: a pathologically distinct 4R tauopathy. *Nat Rev Neurol*. 2011;7:263–272.
53. Zhang W et al. Novel tau filament fold in corticobasal degeneration. *Nature*. 2020;580:283–287.
54. Zhang H, Cao Y, Ma L, Wei Y, Li H. Possible mechanisms of tau spread and toxicity in Alzheimer's disease. *Front Cell Dev Biol*. 2021;9. https://doi.org/10.3389/fcell.2021.707268.
55. Merezhko M, Uronen RL, Huttunen HJ. The cell biology of tau secretion. *Front Mol Neurosci*. 2020;13. https://doi.org/10.3389/fnmol.2020.569818.
56. Dickson DW. Neuropathology of Pick's disease. *Neurology*. 2001;56(suppl. 4): S16–S20.
57. Williams DR, Lees AJ. Progressive supranuclear palsy: clinicopathological concepts and diagnostic challenges. *Lancet Neurol*. 2009;8:270–279.
58. Brunello CA, Merezhko M, Uronen RL, Huttunen HJ. Mechanisms of secretion and spreading of pathological tau protein. *Cell Mol Life Sci*. 2020;77:1721–1744.
59. Kouri N et al. Neuropathological features of corticobasal degeneration presenting as corticobasal syndrome or Richardson syndrome. *Brain*. 2011;134:3264–3275.
60. Scheres SH, Zhang W, Falcon B, Goedert M. Cryo-EM structures of tau filaments. *Curr Opin Struct Biol*. 2020;64:17–25.
61. Shi Y, Ghetti B, Goedert M, Scheres SHW. Cryo-EM structures of chronic traumatic encephalopathy tau filaments with PET ligand flortaucipir. *J Mol Biol*. 2023;435, 168025.
62. Lippens G, Gigant B. Elucidating Tau function and dysfunction in the era of cryo-EM. *J Biol Chem*. 2019;294:9316–9325.
63. Fitzpatrick AW et al. Cryo-EM structures of tau filaments from Alzheimer's disease brain. *Nature*. 2017;547:185.
64. Ebashi M et al. How to demix Alzheimer-type and PSP-type tau lesions out of their mixture -hybrid approach to dissect comorbidity. *Acta Neuropathol Commun*. 2019;7:71.
65. Louros N et al. Local structural preferences in shaping tau amyloid polymorphism. *Nat Commun*. 2024;15:1028.
66. Lövestam S et al. Disease-specific tau filaments assemble via polymorphic intermediates. *Nature*. 2024;625:119–125.
67. Wu L et al. Selective detection of misfolded tau from postmortem Alzheimer's disease brains. *Front Aging Neurosci*. 2022;14, 945875.
68. Kyalu Ngoie Zola N et al. Specific post-translational modifications of soluble tau protein distinguishes Alzheimer's disease and primary tauopathies. *Nat Commun*. 2023;14:3706.
69. Bisi N, Pinzi L, Rastelli G, Tonali N. Early diagnosis of neurodegenerative diseases: what has been undertaken to promote the transition from PET to fluorescence tracers. *Molecules*. 2024;29:722.
70. Coakeley S et al. Positron emission tomography imaging of tau pathology in progressive supranuclear palsy. *J Cereb Blood Flow Metab*. 2017;37:3150–3160.
71. Fleisher AS et al. Positron emission tomography imaging with [18F]flortaucipir and postmortem assessment of Alzheimer disease neuropathologic changes. *JAMA Neurol*. 2020;77:829–839.
72. Badachhape A et al. A novel MRI contrast agent for identifying hyperphosphorylative neurons as a marker of future tau pathology. *Alzheimer's Dementia*. 2020;16(suppl. 5)e041080.
73. Cui M, Ono M, Watanabe H, Kimura H, Liu B, Saji H. Smart near-infrared fluorescence probes with donor–acceptor structure for in vivo detection of β-amyloid deposits. *J Am Chem Soc*. 2014;136:3388–3394.
74. Fu H et al. Highly sensitive near-infrared fluorophores for in vivo detection of amyloid-β plaques in Alzheimer's disease. *J Med Chem*. 2015;58:6972–6983.
75. Oh Y, Lee TG, Kim MK, Chong Y. Thiophene-π-cyanoacetamides show intense and tau-selective turn-on fluorescence in the near-infrared region. *Bull Kor Chem Soc*. 2021;42:1285–1288.
76. Raymond SB, Skoch J, Hills ID, Nesterov EE, Swager TM, Bacskai BJ. Smart optical probes for near-infrared fluorescence imaging of Alzheimer's disease pathology. *Eur J Nucl Med Mol Imaging*. 2008;35(suppl. 1):S93–S98.
77. Selkoe DJ, Hardy J. The amyloid hypothesis of Alzheimer's disease at 25 years. *EMBO Mol Med*. 2016;8:595–608.
78. Ganguly P et al. Tau assembly: the dominant role of PHF6 (VQIVYK) in microtubule binding region repeat R3. *J Phys Chem B*. 2015;119:4582–4593.
79. Arakhamia T et al. Posttranslational modifications mediate the structural diversity of tauopathy strains. *Cell*. 2020;180:633–644.

80. Xia CF et al. [(18)F]T807, a novel tau positron emission tomography imaging agent for Alzheimer's disease. *Alzheimers Dement*. 2013;9:666–676.
81. Wood H. [11C]PBB3—a new PET ligand that identifies tau pathology in the brains of patients with AD. *Nat Rev Neurol*. 2013;9:599.
82. Koga S, Ono M, Sahara N, Higuchi M, Dickson DW. Fluorescence and autoradiographic evaluation of tau PET ligand PBB3 to α-synuclein pathology. *Mov Disord*. 2017;32:884–892.
83. Maruyama M et al. Imaging of tau pathology in a tauopathy mouse model and in Alzheimer patients compared to normal controls. *Neuron*. 2013;79:1094–1108.
84. Lemoine L et al. Comparative binding properties of the tau PET tracers THK5117, THK5351, PBB3, and T807 in postmortem Alzheimer brains. *Alzheimer's Res Therapy*. 2017;9:96.
85. Malarte ML, Nordberg A, Lemoine L. Characterization of MK6240, a tau PET tracer, in autopsy brain tissue from Alzheimer's disease cases. *Eur J Nucl Med Mol Imaging*. 2020;48:1093.
86. Hostetler ED et al. Preclinical characterization of 18F-MK-6240, a promising PET tracer for in vivo quantification of human neurofibrillary tangles. *J Nucl Med*. 2016;57:1599–1606.
87. Aguero C et al. Head-to-head comparison of [18F]-Flortaucipir, [18F]-MK-6240 and [18F]-PI-2620 postmortem binding across the spectrum of neurodegenerative diseases. *Acta Neuropathol*. 2024;147:25.
88. Chien DT et al. Early clinical PET imaging results with the novel PHF-tau radioligand [F18]-T808. *J Alzheimers Dis*. 2014;38:171–184.
89. Honer M et al. Preclinical evaluation of 18F-RO6958948, 11C-RO6931643, and 11C-RO6924963 as novel PET radiotracers for imaging tau aggregates in Alzheimer disease. *J Nucl Med*. 2018;59:675–681.
90. Malarte ML, Gillberg PG, Kumar A, Bogdanovic N, Lemoine L, Nordberg A. Discriminative binding of tau PET tracers PI2620, MK6240 and RO948 in Alzheimer's disease, corticobasal degeneration and progressive supranuclear palsy brains. *Mol Psychiatry*. 2023;28:1272–1283.
91. Tezuka T et al. Evaluation of [18F]PI-2620, a second-generation selective tau tracer, for assessing four-repeat tauopathies. *Brain Commun*. 2021;3, fcab190.
92. Shi Y et al. Cryo-EM structures of tau filaments from Alzheimer's disease with PET ligand APN-1607. *Acta Neuropathol*. 2021;141:697–708.
93. Tagai K et al. An optimized reference tissue method for quantification of tau protein depositions in diverse neurodegenerative disorders by PET with 18F-PM-PBB3 (18F-APN-1607). *Neuroimage*. 2022;264, 119763.
94. Merz GE et al. Stacked binding of a PET ligand to Alzheimer's tau paired helical filaments. *Nat Commun*. 2023;14:3048.
95. Lois C, Gonzalez I, Johnson KA, Price JC. PET imaging of tau protein targets: a methodology perspective. *Brain Imaging Behav*. 2019;13:333–344.
96. Teng E et al. Cross-sectional associations between [18F]GTP1 tau PET and cognition in Alzheimer's disease. *Neurobiol Aging*. 2019;81:138–145.
97. Baker SL et al. Evaluation of [18F]-JNJ-64326067-AAA tau PET tracer in humans. *J Cereb Blood Flow Metab*. 2021;41:3302–3313.
98. Declercq L et al. Preclinical evaluation of 18F-JNJ64349311, a novel PET tracer for tau imaging. *J Nucl Med*. 2017;58:975–981.
99. Harada R et al. Preclinical characterization of the tau PET tracer [18F]SNFT-1: comparison of tau PET tracers. *J Nucl Med*. 2023;64:1495–1501.
100. Walji AM et al. Discovery of 6-(fluoro-18F)-3-(1H-pyrrolo[2,3-c]pyridin-1-yl) isoquinolin-5-amine ([18F]-MK-6240): a positron emission tomography (PET) imaging agent for quantification of neurofibrillary tangles (NFTs). *J Med Chem*. 2016;59:4778–4789.
101. Brendel M et al. Assessment of 18F-PI-2620 as a biomarker in progressive supranuclear palsy. *JAMA Neurol*. 2020;77:1408–1419.
102. Kroth H et al. Discovery and preclinical characterization of [18F]PI-2620, a next-generation tau PET tracer for the assessment of tau pathology in Alzheimer's disease and other tauopathies. *Eur J Nucl Med Mol Imaging*. 2019;46:2178–2189.
103. Wang Y, Cai L, Zhou K, Cui M, Yao S. Biodistribution and dosimetry evaluation for a novel tau tracer [18F]-S16 in healthy volunteers and its application in assessment of tau pathology in Alzheimer's disease. *Front Bioeng Biotechnol*. 2022;9. https://doi.org/10.3389/fbioe.2021.812818.
104. Lindberg A et al. Radiosynthesis, in vitro and in vivo evaluation of [18F]CBD-2115 as a first-in-class radiotracer for imaging 4R-tauopathies. *ACS Chem Neurosci*. 2021;12:596–602.
105. Okamura N et al. Quinoline and benzimidazole derivatives: candidate probes for in vivo imaging of tau pathology in Alzheimer's disease. *J Neurosci*. 2005;25:10857–10862.
106. Fodero-Tavoletti MT et al. 18F-THK523: a novel in vivo tau imaging ligand for Alzheimer's disease. *Brain*. 2011;134:1089–1100.
107. Harada R et al. Comparison of the binding characteristics of [18F]THK-523 and other amyloid imaging tracers to Alzheimer's disease pathology. *Eur J Nucl Med Mol Imaging*. 2013;40:125–132.
108. Okamura N et al. Novel 18F-labeled arylquinoline derivatives for noninvasive imaging of tau pathology in Alzheimer disease. *J Nucl Med*. 2013;54:1420–1427.
109. Villemagne VL et al. In vivo evaluation of a novel tau imaging tracer for Alzheimer's disease. *Eur J Nucl Med Mol Imaging*. 2014;41:816–826.
110. Okamura N et al. Non-invasive assessment of Alzheimer's disease neurofibrillary pathology using 18F-THK5105 PET. *Brain*. 2014;137:1762–1771.
111. Leinonen V et al. S-[18F]THK-5117-PET and [11C]PIB-PET imaging in idiopathic normal pressure hydrocephalus in relation to confirmed amyloid-β plaques and tau in brain biopsies. *J Alzheimers Dis*. 2018;64:171–179.
112. Ng KP et al. Monoamine oxidase B inhibitor, selegiline, reduces 18F-THK5351 uptake in the human brain. *Alzheimers Res Ther*. 2017;9. https://doi.org/10.1186/s13195-017-0253-y.
113. Carroll EC et al. Methods for high throughput discovery of fluoroprobes that recognize tau fibril polymorphs. *bioRxiv*. 20242024.09.02.610853. https://doi.org/10.1101/2024.09.02.610853.
114. *Handbook of Radiopharmaceuticals*. 1st ed. John Wiley & Sons, Ltd; 2002. https://doi.org/10.1002/0470846380.
115. Wooten DW et al. Pharmacokinetic evaluation of the tau PET radiotracer 18F-T807 (18F-AV-1451) in human subjects. *J Nucl Med*. 2017;58:484–491.
116. Flortaucipir F-18. https://go.drugbank.com/drugs/DB14914.
117. Declercq L et al. Comparison of new tau PET-tracer candidates with [18F]T808 and [18F]T807. *Mol Imaging*. 2016;15, 1536012115624920.
118. Acuff SN, Mathotaarachchi S, Zukotynski K, Osborne D, Subramaniam R. Clinical and technical considerations for brain PET imaging for dementia. *J Nucl Med Technol*. 2020;48:5–8.
119. Rabinovici GD et al. Updated appropriate use criteria for amyloid and tau PET: a report from the Alzheimer's Association and Society for Nuclear Medicine and Molecular Imaging Workgroup. *Alzheimers Dement*. 2025;21, e14338.
120. Miyamoto M et al. Radiation dosimetry and pharmacokinetics of the tau PET tracer florzolotau (18F) in healthy Japanese subjects. *Ann Nucl Med*. 2023;37:300–309.
121. Mohammadi Z, Alizadeh H, Marton J, Cumming P. The sensitivity of tau tracers for the discrimination of Alzheimer's disease patients and healthy controls by PET. *Biomolecules*. 2023;13:290.
122. Li Y, Liu T, Cui M. Recent development in selective Tau tracers for PET imaging in the brain. *Chin Chem Lett*. 2022;33:3339–3348.
123. Marquié M et al. [F-18]-AV-1451 binding correlates with postmortem neurofibrillary tangle Braak staging. *Acta Neuropathol*. 2017;134:619–628.
124. Burnham SC et al. A review of the flortaucipir literature for positron emission tomography imaging of tau neurofibrillary tangles. *Brain Commun*. 2024;6, fcad305.
125. Beach TG. A review of biomarkers for neurodegenerative disease: will they swing us across the valley? *Neurol Ther*. 2017;6(suppl. 1):5–13.
126. Marquié M et al. Lessons learned about [F-18]-AV-1451 off-target binding from an autopsy-confirmed Parkinson's case. *Acta Neuropathol Commun*. 2017;5:75.
127. Wright JP et al. Monoamine oxidase binding not expected to significantly affect [18F]flortaucipir PET interpretation. *Eur J Nucl Med Mol Imaging*. 2022;49:3797–3808.
128. Murugan NA, Nordberg A, Ågren H. Different positron emission tomography tau tracers bind to multiple binding sites on the tau fibril: insight from computational modeling. *ACS Chem Neurosci*. 2018;9:1757–1767.
129. Zhou Y, Li J, Nordberg A, Ågren H. Dissecting the binding profile of PET tracers to corticobasal degeneration tau fibrils. *ACS Chem Neurosci*. 2021;12:3487–3496.
130. Murugan NA, Nordberg A, Ågren H. Cryptic sites in tau fibrils explain the preferential binding of the AV-1451 PET tracer toward Alzheimer's tauopathy. *ACS Chem Neurosci*. 2021;12:2437–2447.
131. Li J, Kumar A, Långström B, Nordberg A, Ågren H. Insight into the binding of first- and second-generation PET tracers to 4R and 3R/4R tau protofibrils. *ACS Chem Neurosci*. 2023;14:3528–3539.
132. Sanabria Bohórquez S et al. [18F]GTP1 (Genentech Tau Probe 1), a radioligand for detecting neurofibrillary tangle tau pathology in Alzheimer's disease. *Eur J Nucl Med Mol Imaging*. 2019;46:2077–2089.
133. Ravikumar S et al. Postmortem imaging reveals patterns of medial temporal lobe vulnerability to tau pathology in Alzheimer's disease. *Nat Commun*. 2024;15:4803.
134. Josephs KA et al. Flortaucipir PET uncovers relationships between tau and amyloid-β in primary age-related tauopathy and Alzheimer's disease. *Sci Transl Med*. 2024;16, eado8076.

135. Marquié M et al. Validating novel tau positron emission tomography tracer [F-18]-AV-1451 (T807) on postmortem brain tissue. *Ann Neurol*. 2015;78:787–800.
136. Choi JY et al. Off-target 18F-AV-1451 binding in the basal ganglia correlates with age-related iron accumulation. *J Nucl Med*. 2018;59:117–120.
137. Gogola A et al. Direct comparison of the Tau PET tracers 18F-flortaucipir and 18F-MK-6240 in human subjects. *J Nucl Med*. 2022;63:108–116.
138. Tagai K et al. High-contrast in vivo imaging of tau pathologies in Alzheimer's and non-Alzheimer's disease tauopathies. *Neuron*. 2021;109:42–58.
139. Seidler PM et al. Structure-based discovery of small molecules that disaggregate Alzheimer's disease tissue derived tau fibrils in vitro. *Nat Commun*. 2022;13:5451.
140. Tao Y et al. Structural mechanism for specific binding of chemical compounds to amyloid fibrils. *Nat Chem Biol*. 2023;19:1235–1245.
141. Smith MS et al. Docking for molecules that bind in a symmetric stack with SymDOCK. *J Chem Inf Model*. 2024;64:425–434.
142. Kunach P et al. Cryo-EM structure of Alzheimer's disease tau filaments with PET ligand MK-6240. *Nat Commun*. 2024;15:8497.
143. Mishra SK, Yamaguchi Y, Higuchi M, Sahara N. Pick's tau fibril shows multiple distinct PET probe binding sites: insights from computational modelling. *Int J Mol Sci*. 2021;22:349.
144. Wood H. Alzheimer disease: [11C]PBB3–a new PET ligand that identifies tau pathology in the brains of patients with AD. *Nat Rev Neurol*. 2013;9:599.
145. Brendel M et al. [18F]-THK5351 PET correlates with topology and symptom severity in progressive supranuclear palsy. *Front Aging Neurosci*. 2018;9. https://doi.org/10.3389/fnagi.2017.00440.
146. Su Y et al. Tau PET imaging with [18F]PM-PBB3 in frontotemporal dementia with MAPT mutation. *J Alzheimers Dis*. 2020;76:149–157.
147. Weng CC et al. Characterization of 18F-PM-PBB3 (18F-APN-1607) uptake in the rTg4510 mouse model of tauopathy. *Molecules*. 2020;25:1750.
148. Endo H et al. A machine learning–based approach to discrimination of tauopathies using [F]PM-PBB3 PET images. *Mov Disord*. 2022;37:2236–2246.
149. Nakano Y et al. PET-based classification of corticobasal syndrome. *Parkinsonism Relat Disord*. 2022;98:92–98.
150. Villemagne VL, Fodero-Tavoletti MT, Masters CL, Rowe CC. Tau imaging: early progress and future directions. *Lancet Neurol*. 2015;14:114–124.
151. Yeo SK, Shepelytskyi Y, Grynko V, Albert MS. Molecular imaging of fluorinated probes for tau protein and amyloid-β detection. *Molecules*. 2020;25:3413.
152. McMurray L et al. Synthesis and assessment of novel probes for imaging tau pathology in transgenic mouse and rat models. *ACS Chem Neurosci*. 2021;12:1885–1893.
153. Dan A et al. Extensive deamidation at asparagine residue 279 accounts for weak immunoreactivity of tau with RD4 antibody in Alzheimer's disease brain. *Acta Neuropathol Commun*. 2013;1:54.
154. Vermeiren C et al. The tau positron-emission tomography tracer AV-1451 binds with similar affinities to tau fibrils and monoamine oxidases. *Mov Disord*. 2018;33:273–281.
155. Foster K et al. Preclinical characterization and IND-enabling safety studies for PNT001, an antibody that recognizes cis-pT231 tau. *Alzheimers Dement*. 2023;19:4662–4674.
156. Luca W, Foster K, McClure K, Ahlijanian MK, Jefson M. A phase 1 single-ascending-dose trial in healthy volunteers to evaluate the safety, tolerability, pharmacokinetics, and immunogenicity of intravenous PNT001, a novel mid-domain tau antibody targeting cis-pT231 tau. *J Prev Alzheimers Dis*. 2024;11:366–374.
157. Wagner J et al. Reducing tau aggregates with anle138b delays disease progression in a mouse model of tauopathies. *Acta Neuropathol*. 2015;130:619–631.
158. Deeg AA et al. Anle138b and related compounds are aggregation specific fluorescence markers and reveal high affinity binding to α-synuclein aggregates. *Biochim Biophys Acta*. 2015;1850:1884–1890.
159. Tian M et al. International consensus on the use of tau PET imaging agent 18F-flortaucipir in Alzheimer's disease. *Eur J Nucl Med Mol Imaging*. 2022;49:895–904.
160. Harada R et al. 18F-THK5351: a novel PET radiotracer for imaging neurofibrillary pathology in Alzheimer disease. *J Nucl Med*. 2016;57:208–214.
161. Zdrazil B et al. The ChEMBL Database in 2023: a drug discovery platform spanning multiple bioactivity data types and time periods. *Nucleic Acids Res*. 2024;52:D1180–D1192.
162. Berman HM et al. The Protein Data Bank. *Nucleic Acids Res*. 2000;28:235–242.
163. Liu T, Lin Y, Wen X, Jorissen RN, Gilson MK. BindingDB: a web-accessible database of experimentally determined protein–ligand binding affinities. *Nucleic Acids Res*. 2007;35(suppl. 1):D198–D201.
164. Chopra A et al. Molecular imaging and contrast agent database (MICAD): evolution and progress. *Mol Imaging Biol*. 2012;14:4–13.